MONOTONE METHODS ON NON-MATCHING GRIDS FOR NON LINEAR CONTACT PROBLEMS

BARBARA I. WOHLMUTH* AND ROLF H. KRAUSE†

Abstract. Nonconforming domain decomposition techniques provide a powerful tool for the numerical approximation of partial differential equations. We use a generalized mortar method based on dual Lagrange multipliers for the discretization of a non linear contact problem between linear elastic bodies. In the case of unilateral contact problems, pointwise constraints occur and monotone multigrid methods yield efficient iterative solvers. Here, we generalize these techniques to non-matching triangulations where the constraints are realized in terms of weak integral conditions. The basic new idea is the construction of a nested sequence of nonconforming constrained spaces. We use suitable basis transformations and a multiplicative correction. In contrast to other approaches, no outer iteration scheme is required. The resulting monotone method is of optimal complexity and can be implemented as a multigrid method. Numerical results illustrate the performance of our approach in 2D and 3D.

Key words. contact problems, dual space, linear elasticity, monotone methods, mortar finite elements, multigrid methods, non-matching triangulations

AMS subject classifications. 65N30, 65N55, 74B10

1. Introduction. During the last decades, the interest in the numerical simulation of contact problems has lead to an increased research activity in this area, see, e.g., [13, 16, 17, 38] and [23, 24, 42] for survey papers. Unfortunately, the numerical simulation of contact problems turns out to be difficult. The non penetration condition between the bodies coming into contact gives rise to an unknown contact zone depending non linearly on the displacements. By means of suitable inequality constraints which model the non penetration condition, non linear and non differentiable problems arise. Thus, standard Newton methods cannot be applied directly.

Often, active set strategies [1, 11, 15, 21, 22] are used. Here, the actual contact set is iterated and within each iteration step one linear problem with a given contact zone has to be solved. Also widely used for the numerical simulation of contact problems are penalty methods. They are based on regularization and give rise to a non linear but differentiable regularized energy functional. In the case of a multi body contact problem, penalty methods can be combined with contact elements working on non-matching triangulations, see, e.g., [12, 37, 43]. The advantage of penalty methods is that they can be implemented in a straightforward way. However, the quality of the numerical solution depends strongly on the penalty parameter.

For one-sided contact problems, monotone multigrid methods yield globally convergent and efficient iterative solvers, see [28, 30, 31]. These methods are based on the minimization of the non linear energy functional and do not depend on a penalty parameter. Monotone multigrid methods can be implemented as a modification of a standard linear multigrid cycle and provide multigrid efficiency for one-sided contact problems. Unfortunately, these techniques cannot be applied directly to multi body contact problems. This is caused by the nonconforming situation at the interface between the bodies. On the discrete level, the meshes of the bodies cannot be expected to match. Since the accuracy of the numerical solution depends strongly on the discretization of the transmission conditions, the choice of the discrete transfer operator is of crucial importance for the whole discretization scheme. A stable as well as efficient discretization of the transmission conditions at the interface can be provided by mortar methods. Originally introduced for linear problems in the context of nonconforming domain decomposition techniques in [6], they have also been applied to contact problems, see, e.g., [4, 10, 20].

*Math. Institut A, Universität Stuttgart, Pfaffenwaldring 57, D–70569 Stuttgart, Germany.
wohlmuth@mathematik.uni-stuttgart.de, http://www.mathematik.uni-stuttgart.de/mathA/lst7

† Institut für Mathematik I, Freie Universität Berlin, Arnimallee 2, D–14195 Berlin, Germany
krause@math.fu-berlin.de, http://www.math.fu-berlin.de/~krause

In this paper, we present a new monotone multigrid method which does not require any regularization of the non differentiability and which uses mortar techniques for the information transfer at the interface. In that way, we obtain not only a globally convergent method but also optimal estimates for the discretization error. The resulting new approach for the efficient numerical simulation of multi body contact problems is based on the combination of monotone multigrid techniques, [30, 31], dual mortar methods, [6, 7, 41], a suitable basis transformation and a new sequence of nested nonconforming finite element spaces. Here in contrast to [4, 10, 20], we use dual Lagrange multipliers yielding locally defined basis functions. Dual Lagrange multipliers yield the same accuracy as standard multipliers but give rise to a more efficient realization of the transfer operator. In particular, no mass matrix has to be inverted at the interface.

Our new iterative solver is globally convergent and of optimal complexity. It requires only one suitable basis transformation and can be realized in terms of a standard multigrid method and local pre- and postprocessing steps. Thus, it can be implemented as a modification of a standard linear geometric or algebraic multigrid method. Moreover, optimal a priori estimates for the boundary stresses which play the role of a Lagrange multiplier are available. The approach is very flexible and can be easily generalized to contact problems including friction. Particularly, the method does not rely on a penalty parameter and no outer iteration is required. We also emphasize that once the discrete contact boundary has been identified, our new method reduces to a linear subspace correction method.

The rest of this paper is organized as follows: In Section 2, we introduce the non linear contact problem, and we formulate the discrete non penetration condition in terms of weak integral inequalities using dual Lagrange multipliers. In Section 3, we introduce a suitable basis transformation and decompose the global non linear problem in a global linear and local non linear subproblems. In Section 4, we provide a nested sequence of nonconforming spaces and introduce modified prolongation and restriction operators. In terms of these modifications, we can define our new monotone multigrid method. Finally in Section 5, numerical results in 2D and 3D are shown illustrating the efficiency and flexibility of our new algorithm.

2. A non linear contact problem. In this section, we consider a nonconforming approach for the elastic contact between deformable bodies. The discretization is based on mortar finite element techniques using dual Lagrange multipliers. A similar formulation in terms of standard Lagrange multipliers can be found in [5, 20].

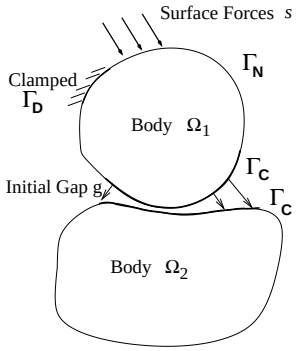

FIG. 2.1. *Two body contact problem and decomposition into* Γ_D, Γ_N *and* Γ_C

For simplicity, we restrict ourselves to the case of two deformable bodies in contact. The two bodies in their reference configuration are identified with the domains $\Omega_k \subset \mathbb{R}^d$, $k \in \{s, m\}$, $d = 2, 3$, and we decompose the solution $\mathbf{u}$ in $\mathbf{u} = (\mathbf{u}_1, \mathbf{u}_m)$, and write $(\mathbf{u}_k)_n := \mathbf{u}_k \cdot \mathbf{n}_k$, $k \in \{s, m\}$, where $\mathbf{n}_k$ is the outer unit normal on $\partial\Omega_k$. The non-mortar side is associated with subdomain Ω_s and the mortar side with the domain Ω_m. The subscript s is motivated by the non-mortar side playing the role of a "slave" side.

Correspondingly, quantities on the mortar or "master" side are being attached by the subscript m. We start with the decomposition of the boundary of Ω into three disjoint parts, Γ_D is the Dirichlet part, Γ_N denotes the Neumann part and Γ_C stands for the contact boundary, see Figure 2.1.

On both subdomains, the possible contact boundary Γ_C is associated with a suitable parametrization. The actual contact zone between the two bodies is a priori unknown and is assumed to be a subset of Γ_C. We denote tensor and vector quantities by bold symbols, e.g., $\boldsymbol{\tau}$ and $\mathbf{v}$, and its components by τ_{ij} and v_i, $1 \leq i, j \leq d$. The partial derivative with respect to x_j is abbreviated with the index $_{,j}$. Furthermore, we enforce the summation convention on all repeated indices ranging from 1 to d, and we denote by δ_{ij} the Kronecker symbol.

The non linear contact problem can be written as a boundary value problem. Here, we consider the case without friction. In addition to the equilibrium conditions in Ω_s and Ω_m and the boundary conditions on $\partial\Omega$

$$\begin{array}{rcll} -\sigma_{ij}(\mathbf{u})_{,j} & = & f_i, & \text{in } \Omega_s \cup \Omega_m \ , \\ \mathbf{u} & = & 0, & \text{on } \Gamma_D \ , \\ \sigma_{ij}(\mathbf{u}) \cdot n_j & = & p_i, & \text{on } \Gamma_N \ , \end{array} \tag{2.1}$$

we have the following conditions on the possible contact boundary Γ_C

$$\begin{array}{rcccl} \boldsymbol{\sigma}_T(\mathbf{u}_s) & = & \boldsymbol{\sigma}_T(\mathbf{u}_m) & = & 0 \ , \\ \sigma_n(\mathbf{u}_s) & = & \sigma_n(\mathbf{u}_m) & \leq & 0 \ , \end{array} \tag{2.2}$$

and the linearized contact condition on Γ_C

$$\begin{array}{rcl} g & \geq & (\mathbf{u}_s)_n + (\mathbf{u}_m)_n \ , \\ 0 & = & ((\mathbf{u}_s)_n + (\mathbf{u}_m)_n - g)\, \sigma_n(\mathbf{u}_s) \ , \end{array} \tag{2.3}$$

where the function $g\colon \Gamma_C \subset \mathbb{R}^d \longrightarrow \mathbb{R}$ is the distance between the two bodies in normal direction taken with respect to the reference configuration; see, e.g., [8, 16]. We assume that g is continuous. The system (2.1) is obtained by the equation of equilibrium, the strain-displacement relation and the constitutive law. We refer to [24] for an introduction to linear elasticity. In the case of a linear elastic material, the stress tensor $\boldsymbol{\sigma}$ depends linearly on the infinitesimal strain tensor $\boldsymbol{\epsilon}(\mathbf{u}) := 1/2(\nabla\mathbf{u} + \nabla\mathbf{u}^T)$. The stress tensor $\boldsymbol{\sigma}$ is given by Hooke's law

$$\sigma_{ij}(\mathbf{u}) := E_{ijlm}\, u_{l,m} \ ,$$

where Hooke's tensor $\mathbf{E} := (E_{ijlm})_{ijlm=1}^d$, $E_{ijlm} \in L^\infty(\Omega)$, is assumed to be sufficiently smooth, symmetric and uniformly positive definite. In the case of a homogeneous isotropic material, Hooke's tensor has the simple form

$$E_{ijlm} = \frac{E\ \nu}{(1+\nu)(1-2\nu)}\delta_{ij}\delta_{kl} + \frac{E}{2(1+\nu)}(\delta_{ik}\delta_{jl} + \delta_{il}\delta_{jk}) \ ,$$

where $E > 0$ is Young's modulus and $\nu \in (0, 1/2)$ is the Poisson ratio. Figure 2.2 illustrates the normal stress at the contact boundary.

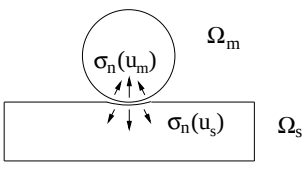

FIG. 2.2. *Normal stress at the contact boundary*

Since no friction occurs, the tangential component of the stress tensor vanishes at the contact boundary, and is set to zero in the first equation of (2.2). We have only contact pressure at Γ_C. If there is no contact between the two bodies, the boundary stresses at Γ_C are zero; see (2.2) and (2.3). The bilinear form $a(\cdot,\cdot)$ is defined by

$$a(\mathbf{v},\mathbf{w}) := \sum_{k=1}^{2} \int_{\Omega_k} E_{ijlm} w_{i,j} v_{l,m}\, dx, \quad \mathbf{w},\mathbf{v} \in \prod_{k=1}^{2} \mathbf{H}^1(\Omega_k) \ ,$$

where E_{ijlm} is assumed to be constant on each subdomain and $\mathbf{H}^1(\Omega_k) := (H^1(\Omega_k))^d$. We write $f(\mathbf{v}) := (\mathbf{v},\mathbf{f})_{0;\Omega} + (\mathbf{v},\mathbf{p})_{0;\Gamma_N}$ and denote by $f_k(\cdot)$ and $a_k(\cdot,\cdot)$ the restriction of $f(\cdot)$ and $a(\cdot,\cdot)$ to Ω_k , $k \in \{s,m\}$, respectively.

The weak solution of the non linear contact problem can be obtained by a minimization problem on a convex set $\mathcal{K}$. We define the set of admissible displacements by

$$\mathcal{K} := \{\mathbf{v} \in \mathbf{X} \mid (\mathbf{v}_s)_n + (\mathbf{v}_m)_n \le g\} \ ,$$

where $\mathbf{X} := \mathbf{H}^1_*(\Omega_s) \times \mathbf{H}^1_*(\Omega_m)$ and $\mathbf{H}^1_*(\Omega_k) \subset \mathbf{H}^1(\Omega_k)$ satisfies homogeneous Dirichlet boundary conditions on $\partial\Omega_k \cap \Gamma_D$, $k \in \{s,m\}$. Then, the weak solution of (2.1)–(2.3) is defined by: Find $\mathbf{u} \in \mathcal{K}$ such that

$$J(\mathbf{u}) \le \min_{\mathbf{v}\in\mathcal{K}} J(\mathbf{v}) \ , \tag{2.4}$$

where the energy functional $J(\cdot)$ is given by $J(\mathbf{v}) := \frac{1}{2}a(\mathbf{v},\mathbf{v}) - f(\mathbf{v})$ on $\mathcal{K}$; see, e.g., [8, 16]. The minimization problem (2.4) is equivalent to a variational inequality: Find $\mathbf{u} \in \mathcal{K}$ such that

$$a(\mathbf{u},\mathbf{v}-\mathbf{u}) \ge f(\mathbf{v}-\mathbf{u}), \qquad \mathbf{v} \in \mathcal{K} \ . \tag{2.5}$$

In the rest of this section, we consider a saddle point formulation of (2.5). To do so, we introduce a Lagrange multiplier space $\mathbf{M} := M^d$. More precisely, we use the dual space of the trace space $\mathbf{W} := W^d$ of $\mathbf{H}^1_*(\Omega_s)$ restricted to Γ_C. Here, we assume that Γ_C is compact embedded in $\partial\Omega_s \setminus \Gamma_D$ or that $g \in H^{1/2}_{00}(\Gamma_C)$. We note that if $\partial\Omega_s \cap \Gamma_N = \emptyset$ then $\mathbf{M} = \mathbf{H}^{-1/2}(\Gamma_C) = (\mathbf{H}^{1/2}_{00}(\Gamma_C))^*$.

Then (2.5) can be rewritten as: Find $(\mathbf{u},\boldsymbol{\lambda}) \in (\mathbf{X},\mathbf{M}^+)$

$$\begin{aligned} a(\mathbf{u},\mathbf{v}) + b(\boldsymbol{\lambda},\mathbf{v}) &= f(\mathbf{v}), & \mathbf{v} &\in \mathbf{X}, \\ b(\boldsymbol{\mu},\mathbf{u}) &\le \langle \boldsymbol{\mu}\cdot\mathbf{n}_s, g\rangle_{\Gamma_C}, & \boldsymbol{\mu} &\in \mathbf{M}^+, \end{aligned} \tag{2.6}$$

where $\mathbf{M}^+ := \{\boldsymbol{\mu} \in \mathbf{M} \mid \langle \boldsymbol{\mu}\cdot\mathbf{n}_s, w\rangle_{\Gamma_C} \ge 0, w \in W^+\}$, $W^+ := \{w \in W \mid w \ge 0\}$. The bilinear form $b(\cdot,\cdot)$ is defined by

$$b(\boldsymbol{\mu},\mathbf{v}) := \langle (\mathbf{v}_s)_n + (\mathbf{v}_m)_n, \boldsymbol{\mu}\cdot\mathbf{n}_s\rangle_{\Gamma_C} \ ,$$

and $\langle\cdot,\cdot\rangle_{\Gamma_C}$ denotes the duality pairing between M and W. From the second inequality in (2.6), we find $\mathbf{u} \in \mathcal{K}$. The variational inequalities (2.5) and (2.6) form the starting point for our discrete approach.

On each subdomain, we use a shape regular triangulation and lowest order conforming finite elements, i.e., piecewise linear finite elements on simplicial triangulations and piecewise bilinear and bicubic elements on rectangular and hexahedral triangulations, respectively. The finite element spaces associated with Ω_s and Ω_m satisfying homogeneous Dirichlet boundary conditions on Γ_D are denoted by $X_{s;h_s}$ and $X_{m;h_m}$, respectively. Additionally, we introduce a discrete Lagrange multiplier space M_h being defined on the non-mortar side of the possible contact boundary Γ_C. The discrete trace space of $X_{s;h_s}$ on the non-mortar side is denoted by W_h. We assume that Γ_C can be written as the union

of faces and edges in 3D and 2D, respectively. The corresponding discrete spaces for the d-dimensional vector fields are denoted by bold characters $\mathbf{X}_{s;h_s} := X^d_{s;h_s}$, $\mathbf{X}_{m;h_m} := X^d_{s;h_m}$, $\mathbf{X}_h := \mathbf{X}_{s;h_s} \times \mathbf{X}_{m;h_m}$, $\mathbf{W}_h := W^d_h$ and $\mathbf{M}_h := M^d_h$. Here, we use dual Lagrange multiplier spaces. For mortar finite element discretizations dual Lagrange multiplier spaces have been analyzed in [39] and generalized in [25, 34, 40].

For convenience, we recall the characteristic properties of the dual basis functions $\psi_q \in M_h$ associated with the vertices q on the non-mortar side of $\overline{\Gamma}_C$. We note that in contrast to the standard mortar approach no modifications of ψ_q near the boundary of Γ_C are necessary. We denote the standard nodal hat functions associated with the vertices q on the non-mortar side $\partial\Omega_s \cap \overline{\Gamma}_C$ by ϕ^s_q. The set of vertices on the non-mortar side $\partial\Omega_s \cap \overline{\Gamma}_C$ is called $\mathcal{P}_{C;h_s}$. We briefly recall the characteristic properties of our dual basis functions $\psi_q \in M_h$:

- supp ψ_q = supp ϕ^s_q, $q \in \mathcal{P}_{C;h_s}$,
- ψ_q is piecewise linear or bilinear,
- $\sum_{q \in \mathcal{P}_{C;h_s}} \psi_q = 1$,
- $\int_F \psi_p \, \phi^s_q \, d\sigma = \delta_{pq} \int_F \phi^s_q \, d\sigma$, $p, q \in \mathcal{P}_{C;h_s}$, $F \subset \Gamma_C$, for all boundary faces in 3D and all boundary edges in 2D.

We remark that the last property, in general, does not hold for the dual basis functions constructed in [34]. The last property guarantees the biorthogonality relation

$$\int_{\Gamma_C} \psi_p \, \phi^s_q \, d\sigma = \delta_{pq} \int_{\Gamma_C} \phi^s_q \, d\sigma, \quad p, q \in \mathcal{P}_{C;h_s} \ . \tag{2.7}$$

Other choices of dual Lagrange multiplier spaces are possible. In [40], continuous Lagrange multipliers are constructed which are locally defined and piecewise cubic on simplicial triangulations and piecewise bicubic on hexahedral triangulations.

On both subdomains independent triangulations can be used resulting generally in non-matching triangulations at Γ_C. In that situation, a pointwise matching condition yields a non-optimal discretization scheme, see, e.g., [19] and [20] for numerical results in 2D. However, optimal discretization schemes for non-matching triangulations can be obtained if mortar techniques are applied. The essential idea is to replace a strong pointwise coupling condition by a weaker integral condition. We refer to [3, 6, 7] for an overview of mortar methods in the linear case and to [4, 5, 20] for non linear contact problems. The proof of the discretization error is based on the use of the standard Lagrange multiplier space. We do not use this approach, but point out that the same qualitative results can be obtained for our approach. Then, the discrete variational problems reads as follows: Find $\mathbf{u}_h \in \mathcal{K}_h$ such that

$$a(\mathbf{u}_h, \mathbf{v}_h - \mathbf{u}_h) \ \geq \ f(\mathbf{v}_h - \mathbf{u}_h), \qquad \mathbf{v}_h \in \mathcal{K}_h \ , \tag{2.8}$$

where $\mathbf{X}_h := \mathbf{X}_{s;h_s} \times \mathbf{X}_{m;h_m}$ and $\mathcal{K}_h$ is a suitable discrete approximation of $\mathcal{K}$. We set

$$\mathcal{K}_h \ := \ \{\mathbf{v} \in \mathbf{X}_h \mid \ \int_{\Gamma_C} [\mathbf{v}] \cdot \mathbf{n}_p \ \psi_p \ d\sigma \leq \int_{\Gamma_C} g_h \ \psi_p \ d\sigma, \ \ p \in \mathcal{P}_{C;h_s}\} \ ,$$

where $g_h \in W_h$ and $g_h \geq 0$ is a suitable approximation of g. The discrete normal vector $\mathbf{n}_p$ associated with the vertex p is defined by

$$\mathbf{n}_p := \alpha_p \sum_{F \subset \text{ supp } \psi_p} \mathbf{n}_F | \ F \ | \ ,$$

where $\alpha_p > 0$ such that $\|\mathbf{n}_p\| = 1$, $| \ F \ |$ is the area of F, and $\mathbf{n}_F$ is the outer unit normal vector on F, see Figure 2.3.

We note that, in general, $\mathcal{K}_h$ is not a subspace of $\mathcal{K}$. For convenience of the reader, we review the a priori bounds and the main ideas of the proof, see [20, Theorem 3.1].

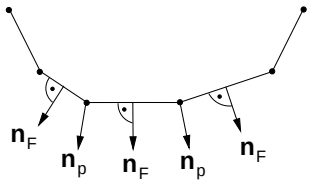

FIG. 2.3. *Outer normal vectors* $\mathbf{n}_F$ *and* $\mathbf{n}_p$

LEMMA 2.1. *Under suitable regularity assumptions on the solution* $\mathbf{u}$ *and the actual contact boundary, we obtain optimal a priori estimates for the discretization error*

$$a(\mathbf{u}-\mathbf{u}_h,\mathbf{u}-\mathbf{u}_h)^{\frac{1}{2}} \leq C(\mathbf{u})(h_s+h_m),$$

where $C(\mathbf{u})$ *does not depend on the meshsize, and* h_s *and* h_m *stand for the meshsize on the non-mortar and mortar side, respectively.*

The proof follows the same lines as given in [20]. However, there are two essential differences. We do not use a subset of the finite element trace space on the non-mortar side to define our Lagrange multiplier space. In contrast to [4, 20], we use a locally defined dual basis to define our Lagrange multiplier space. The second main difference is that we do not use a scalar Lagrange multiplier space but a vector valued one. This modification is motivated by the following observation. The discrete Lagrange multiplier in the mortar setting approximates the boundary stress. In the case of a contact problem, the boundary stress can be decomposed into a scalar component and a vector valued one (scalar in 2D) representing the normal and tangential stresses. If no friction occurs, the tangential stress components are equal to zero and can be therefore eliminated. Then, the Lagrange multiplier space can be defined as an appropriate discrete approximation for the normal stress. However working with a vector valued Lagrange multiplier space is more general, and friction terms can be easily included in the approach. Following [20], it is sufficient to verify a $H^{1/2}$-stability of the mortar projection and to have appropriate approximation properties for the Lagrange multiplier space to obtain the a priori estimate. The stability result for the dual Lagrange multiplier space can be found in [41] and the approximation properties follow by construction from the property $\sum_{p\in\mathcal{P}_{C;h_s}} \psi_p \, d\sigma = 1$.

3. A non linear Gauß–Seidel method. One of the major difficulties in the numerical simulation of contact problems is the non differentiability of the associated energy functional at the contact boundary. Very often regularization techniques; see, e.g., [9, 13], or augmented Lagrangian methods; see, e.g., [33, 35] are used. For multi body contact problems, contact elements can be applied, see, e.g., [43]. Then, the discrete solution depends on a penalty parameter. In [32], a new non linear Dirichlet–Neumann algorithm in combination with mortar techniques has been introduced. It is based on the solution of a linear Neumann problem and a non linear unilateral contact problem in each step. The non linear contact problem is solved by monotone multigrid techniques [28, 29, 30, 31]. Two damping parameters control the convergence of the Dirichlet–Neumann method. If the damping parameters are too small, we observe a slow convergence. On the other hand if the damping parameters are too large, the method does not converge. In 2D, convergence rates which are independent of the refinement level and which are robust with respect to the damping factor can be observed. We refer to [32] for some numerical results illustrating the influence of the damping parameters. However in 3D, the convergence rates depend sensitively on the damping factor. Moreover, the choice of a good damping factor depends extremely on the geometry of the elastic bodies. Figures 3.1 and 3.2 illustrate the influence of the geometry.

In both examples, we use the same parameter setting. The difference is the length of the linear elastic bar which is situated in between of the two cylinders. The two figures show the deformation after 15, 25, 35 and 40 steps of the Dirichlet–Neumann

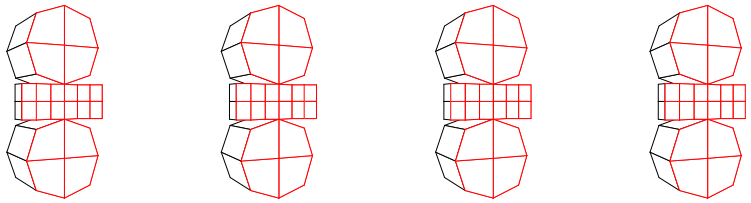

FIG. 3.1. *Convergence of the Dirichlet–Neumann algorithm*

iteration. In case of the short bar, convergence after a few number of iteration steps can be observed. All pictures in Figure 3.1 show the same displacements. The situation is completely different for the long bar. In that case, the method seems to convergence within the first iteration steps but after 30 iteration steps we observe large oscillations, and no convergence can be obtained.

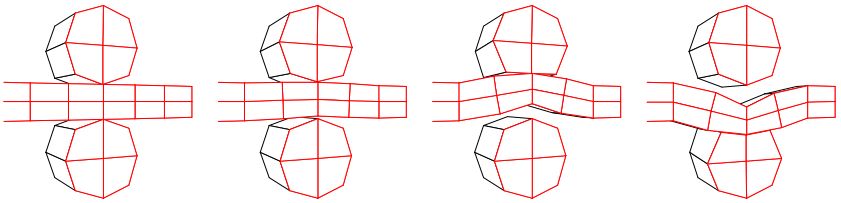

FIG. 3.2. *Oscillation of the Dirichlet–Neumann algorithm*

This observation motivates the introduction of a new monotone method. In particular, the convergence of our new algorithm is guaranteed and does not depend on the choice of a damping parameter. We focus on monotone methods for the iterative solution of the discrete contact problem. In each local iteration step, the solution minimizes the energy with respect to the local search direction and is admissible. An iterate $\mathbf{u}^n$ is called admissible, if it satisfies the constraints at the contact boundary, i.e., if $\mathbf{u}^n \in \mathcal{K}_h$. To do so, we introduce local subspaces $\mathbf{X}_k \subset \mathbf{X}_h$, $1 \leq k \leq K$, and define an iteration sequence $\mathbf{u}^n$ by $\mathbf{u}^{n+1} := \mathbf{u}_K$ and $\mathbf{u}_0 := \mathbf{u}^n$

$$J(\mathbf{u}_k) := \min_{\substack{\mathbf{w}_k \in \mathbf{X}_k \\ \mathbf{u}_{k-1}+\mathbf{w}_k \in \mathcal{K}_h}} J(\mathbf{u}_{k-1} + \mathbf{w}_k), \quad 1 \leq k \leq K \ . \tag{3.1}$$

It is well known [14, 36] that the minimization process (3.1) is equivalent to a non linear block Gauß–Seidel method. Unfortunately to obtain a globally convergent sequence $\mathbf{u}^n$, it is not sufficient to have $\mathbf{X}_h = \mathbf{X}_s + \mathbf{X}_m + \ldots \mathbf{X}_K$.

In the following, we discuss a very simple counterexample and refer to [14, 36] for more details. Let $X := \mathbb{R}^2$, $X_1 := \text{span}\,\{\mathbf{e}_1\}$, $X_2 := \text{span}\,\{\mathbf{e}_2\}$ and the energy functional $J(x_1, x_2) := x_1^2 + x_2^2$. The convex set is defined by $\mathcal{K} := \{(x_1, x_2) \mid x_2 \geq 0, x_1 + x_2 \geq 1\}$. Then it is easy to see that the solution of the minimization problem is $(0.5, 0.5)$. Using $(1, 0)$ as start iterate $\mathbf{x}^0$ and applying the iteration (3.1), we find $\mathbf{x}^n = \mathbf{x}^0$, and we have no convergence. However, if we replace X_2 by span $\{\mathbf{e}_2 - \mathbf{e}_1\}$, we obtain $\mathbf{x}^1 = (0.5, 0.5)$. Figure 3.3 illustrates the parameterization of the convex set $\mathcal{K}$ with respect to the two different choices of subspaces. On the left the convex set is written in terms of $\alpha\mathbf{e}_1 + \beta\mathbf{e}_2$ and on the right in terms of $\alpha\mathbf{e}_1 + \beta(\mathbf{e}_2 - \mathbf{e}_1)$. Theorem 3.1 in [14] yields that the iteration sequence defined by (3.1) converges if the associated parameterization of the convex set has a tensor product structure.

Our algorithm will be based on a suitable basis of the unconstrained product spaces $\mathbf{X}_h$. As we will see, the standard nodal basis of $\mathbf{X}_h$ is not a good choice. The set of all vertices of the triangulations on Ω_s and Ω_m is called $\mathcal{P}_h$. Defining for all vertices p

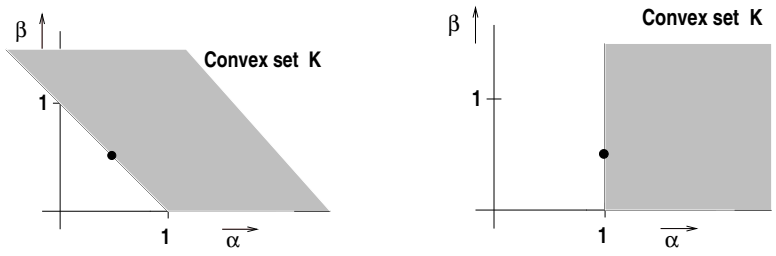

FIG. 3.3. *Parameterizations of the convex set*

the local d-dimensional space $\mathbf{X}_p$ by $\mathbf{X}_p := \{\phi_p \boldsymbol{\alpha} \,|\, \boldsymbol{\alpha} \in \mathbb{R}^d\}$, we find $\mathbf{X}_h = \sum_{p \in \mathcal{P}_h} \mathbf{X}_p$. However, the parameterization of the convex set $\mathcal{K}_h$ with respect to this choice does not have the required tensor product structure. Thus, we cannot expect a convergent scheme. To get a better feeling, we consider the structure of the convex set $\mathcal{K}_h$ in more detail. The constraints can be associated with the nodes on the non-mortar side. For each vertex on the non-mortar side, we have one weak non penetration condition. The biorthogonality of the dual Lagrange multiplier guarantees that the constraints are decoupled. As a consequence, changing the value on the non-mortar side at the vertex $p \in \mathcal{P}_{C;h_s}$ has no influence on the penetration at the vertex $q \in \mathcal{P}_{C;h_s}$, $q \neq p$. To start, let us consider the contact zone. As it is standard in the mortar context, the constraints at the interface are formulated in terms of the Lagrange multiplier space. The algebraic form of the discrete non penetration condition can be written as

$$OD\mathbf{u}^s \leq O\widehat{M}\mathbf{u}^m + \hat{\mathbf{g}} \ , \tag{3.2}$$

where $\mathbf{u}^s$ and $\mathbf{u}^m$ denote the vector representation of the displacement on the non-mortar and mortar side with respect to the standard nodal basis functions, respectively. The components of the vector $\hat{\mathbf{g}}$ are obtained by

$$\hat{g}_p := \int_{\Gamma_C} \psi_p \ g_h \ d\sigma, \quad p \in \mathcal{P}_{C;h_s} \ . \tag{3.3}$$

Due to the use of a dual Lagrange multiplier space, the matrix D is a $dn_s \times dn_s$ diagonal matrix and the matrix $\widehat{M}$ a $dn_s \times dn_m$ mass matrix, where n_s stands for the number of vertices on the non-mortar side and n_m stands for the number of vertices on the mortar side. The block entries of the matrices D and $\widehat{M}$ are given by

$$d_{pp} := \int_{\Gamma_C} \phi_p^s \ d\sigma \ \mathrm{Id}_{d\times d} \ \text{ and } \ \widehat{m}_{pq} := \int_{\Gamma_C} \psi_p \phi_q^m \ d\sigma \ \mathrm{Id}_{d\times d}, \quad p \in \mathcal{P}_{C;h_s}, q \in \mathcal{P}_{C;h_m} \ ,$$

respectively, where $\mathcal{P}_{C;h_m}$ is the set of vertices on the mortar side, i.e., on $\partial\Omega_m \cap \overline{\Gamma}_C$. The additional upper index indicates on which side the nodal hat functions are defined. We recall that the index s stands for the non-mortar side and the index m for the mortar side, i.e., ϕ_q^m is the standard nodal basis function on the mortar side associated with the vertex $q \in \mathcal{P}_{C;h_m}$. Finally, the matrix O is a block diagonal $n_s \times dn_s$ matrix, the entries are given by the row vectors $o_{pp} := \mathbf{n}_p^T$, $p \in \mathcal{P}_{C;h_s}$. Observing that D and O are block diagonal matrices, we find

$$(\mathbf{u}^s)_{\mathbf{n}} := O\mathbf{u}^s \leq OM\mathbf{u}^m + \mathbf{g} \ ,$$

where the components of the vector $\mathbf{g}$ are obtained by $g_p := \hat{g}_p / (\int_{\Gamma_C} \phi_p^s \ d\sigma)$, $p \in \mathcal{P}_{C;h_s}$. The biorthogonality of the basis sets and the locality of the supports yield that $M := D^{-1}\widehat{M}$ is a sparse rectangular mass matrix involving the Lagrange multiplier on the non-mortar side and the basis functions on the mortar side. The duality of the Lagrange

multiplier yields that the constraint (3.2) results in one local constraint for each vertex on the non-mortar side

$$(\mathbf{u}^s)_p \cdot \mathbf{n}_p \leq (M\mathbf{u}^m)_p \cdot \mathbf{n}_p + g_p, \quad p \in \mathcal{P}_{C;h_s} \ . \tag{3.4}$$

We remark that we have by construction $g_p = g_h(p) \geq 0$. Let us start with the case of a non linear Gauß–Seidel method in terms of the standard nodal basis. Then, the Gauß–Seidel method can be carried out locally for all interior nodes and the nodes on the non-mortar side. For each interior node, we solve a linear $d \times d$ system, and for each non-mortar node, we solve a non linear $d \times d$ system with one constraint in normal direction. Unfortunately, the situation for a mortar node is more complex. Solving for each node on the mortar side a local minimization problem does not yield a convergent method. We remark that changing the values $\mathbf{u}_q^m$ at the vertex $q \in \mathcal{P}_{C;h_m}$ on the mortar side influences the non penetration condition at $p \in \mathcal{P}_{C;h_s}$ for p such that $m_{pq} \neq 0$. To obtain a convergent method and to work with nodal basis functions, we have to increase the dimension of $\mathbf{X}_q$, $q \in \mathcal{P}_{C;h_m}$. Enlarging the space $\mathbf{X}_q$ corresponds to increasing the block size in the non linear Gauß–Seidel method. We associate with each nodal point $p^m \in \mathcal{P}_{C;h_m}$ on the mortar side, all nodal points $p^s \in \mathcal{P}_{C;h_s}$ with $p^s \in I_{p^m} := \{q^s \in \mathcal{P}_{C;h_s} \,|\, m_{q^s p^m} \neq 0\}$ on the non-mortar side. The number of vertices n_{p^m} in I_{p^m} reflects the local ratio between the meshsize on the mortar and non-mortar side. Then, a non linear $d(n_{p^m}+1) \times d(n_{p^m}+1)$ problem has to be solved for each nodal point on the mortar side. As long as the block size is small, this can be carried out in an efficient way. However in 3D, unstructured grids result easily in complex block structures, see Figure 3.4. In the right picture all nodes in I_{p^m} are marked with a filled circle. Although the meshsize on mortar and non-mortar side is roughly the same, the resulting non linear system for the mortar node p^m has dimension 54.

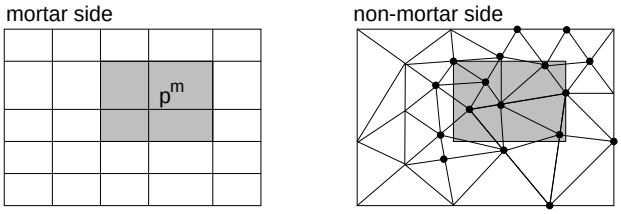

FIG. 3.4. *Unstructured grids on a 2D interface*

If the meshsize on the mortar side is larger than on the non-mortar side, the dimension of the non linear problems which have to be solved can be considerably large. Moreover if we consider a hierarchical multilevel structure on the mortar side, the dimension increases with decreasing refinement level k, more precisely, it is proportional to $2^{(d-1)(L-k)}$ where L is the finest level on the mortar side. Thus working with nodal basis functions for the unconstrained product space is not very efficient in a multigrid context.

Now, the central idea is to modify the nodal basis functions on the mortar side such that the constraint (3.4) can be easily satisfied. One possibility is to replace the nodal hat functions associated with the vertices on the mortar side by the corresponding basis functions of a suitable constrained space $\mathbf{V}_h$. It turns out that a good choice is the nonconforming space of a mortar discretization

$$\mathbf{V}_h := \{\mathbf{v} \in \mathbf{X}_h | \int_{\Gamma_C} [\mathbf{v}] \cdot \boldsymbol{\psi} \, d\sigma = 0, \quad \boldsymbol{\psi} \in \mathbf{M}_h\} \ .$$

We note that in the definition of the space $\mathbf{V}_h$, the normal direction does not enter and that $\mathbf{M}_h$ is a vector valued Lagrange multiplier space. A different possibility to define the space would be to glue only the normal components of the traces together, i.e.,

$$\{\mathbf{v} \in \mathbf{X}_h | \int_{\Gamma_C} [\mathbf{v} \cdot \mathbf{n}_p] \, \psi_p \, d\sigma = 0, \quad p \in \mathcal{P}_{C;h_s}\} \ .$$

Since, we are interested in a general approach which can also handle friction, we do not follow this line. Let us consider an element in $\mathbf{V}_h$ in more detail. The definition of $\mathbf{V}_h$ yields

$$\int_{\Gamma_C} [\mathbf{v}] \cdot \mathbf{n}_p \psi_p \, d\sigma = 0$$

for all vertices p on the non-mortar side. Thus (3.4) is automatically satisfied for all elements in $\mathbf{V}_h$, and $\mathbf{V}_h$ is a subspace of $\mathcal{K}_h$. It can be easily verified that

$$\mathbf{X}_h = \mathbf{V}_h + \sum_{p \in \mathcal{P}_{C;h_s}} \text{span}\,\{\phi_p^s \mathbf{e}_i \,|\, 1 \le i \le d\} =: \mathbf{V}_h + \sum_{p \in \mathcal{P}_{C;h_s}} \mathbf{S}_p \ , \tag{3.5}$$

where $\mathbf{e}_i \in \mathbb{R}^d$ is the i-th. unit vector. Working with the nodal basis of $\mathbf{V}_h$ and the d-dimensional local space $\mathbf{S}_p$, $p \in \mathcal{P}_{C;h_s}$, the non linear block Gauß–Seidel method is extremely easy to realize. In each step, we have to solve a linear $d \times d$ system for each block basis function of $\mathbf{V}_h$. Additionally, we solve for each $\mathbf{S}_p$ a non linear $d \times d$ problem. We point out that the dimension of the non linear subproblems is independent of the triangulations at the interface. In contrast to the nodal basis of $\mathbf{X}_h$, no non linear problem of larger dimension than d has to be solved. Moreover, the number of non linear problems to be solved in each step is the number of vertices on the non-mortar side. This is not the case for the nodal basis of $\mathbf{X}_h$. In that case additionally to the d-dimensional non linear problems associated with the nodal points on the non-mortar side, we have to solve non linear problems associated with the vertices on the mortar side. Moreover, the dimension depends on the meshsize and can be considerably large.

In the rest of this section, we consider the variational problem in more detail to see how the implementation can be realized. We start by introducing a modified basis of $\mathbf{X}_h$ based on the decomposition (3.5). Three different sets of nodes are introduced I_s, I_m and I_i. The sets I_s and I_m stand for the nodes associated with the vertices on non-mortar and mortar side, respectively. The third set I_i contains all remaining nodes. Now, we consider a modified basis Θ of $\mathbf{X}_h$. We obtain Θ from the nodal basis Φ of $\mathbf{X}_h$ by a local basis transformation

$$\Theta := \begin{pmatrix} \Theta_i \\ \Theta_m \\ \Theta_s \end{pmatrix} := \begin{pmatrix} \text{Id} & 0 & 0 \\ 0 & \text{Id} & M^T \\ 0 & 0 & \text{Id} \end{pmatrix} \begin{pmatrix} \Phi_i \\ \Phi_m \\ \Phi_s \end{pmatrix} =: B\Phi \ .$$

Associated with this new basis is the modified stiffness matrix

$$A := \begin{pmatrix} \text{Id} & 0 & 0 \\ 0 & \text{Id} & M^T \\ 0 & 0 & \text{Id} \end{pmatrix} \begin{pmatrix} \hat{A}_{ii} & \hat{A}_{im} & \hat{A}_{is} \\ \hat{A}_{mi} & \hat{A}_{mm} & 0 \\ \hat{A}_{si} & 0 & \hat{A}_{ss} \end{pmatrix} \begin{pmatrix} \text{Id} & 0 & 0 \\ 0 & \text{Id} & 0 \\ 0 & M & \text{Id} \end{pmatrix} = B\widehat{A}B^T \ , \tag{3.6}$$

where $\hat{A}_{kl}$, $k,l \in \{s,m,i\}$, are the block stiffness matrices associated with the nodal basis functions. A straightforward computation shows that A is given as

$$A = \begin{pmatrix} \hat{A}_{ii} & \hat{A}_{im} + \hat{A}_{is}M & \hat{A}_{is} \\ \hat{A}_{mi} + M^T\hat{A}_{si} & \hat{A}_{mm} + M^T\hat{A}_{ss}M & M^T\hat{A}_{ss} \\ \hat{A}_{si} & \hat{A}_{ss}M & \hat{A}_{ss} \end{pmatrix} \ .$$

In terms of the new modified basis, the convergence of our non linear block Gauß–Seidel method is guaranteed, [14, 36]. Moreover, the implementation is extremely easy to realize. In addition to the non linear block Gauß–Seidel method, we have to carry out one pre- and one post processing step. We modify the stiffness matrix according to (3.6) and the right hand side $\hat{f}$ is replaced by f,

$$f := B\hat{f} = \begin{pmatrix} \hat{f}_i \\ \hat{f}_m + M^T\hat{f}_s \\ \hat{f}_s \end{pmatrix} \ .$$

Now, we can apply a non linear Gauß–Seidel method on the modified system. Within each step, we solve for each index $j \in I_i \cup I_m$ a linear $d \times d$ system

$$\mathbf{u}_j = A_{jj}^{-1}(\mathbf{f}_j - \sum_{k \neq j} A_{jk}\,\mathbf{u}_k) \ , \tag{3.7}$$

and for $j \in I_s$ we solve for all $\mathbf{v}_j \ \mathbf{n}_j \leq g_j$

$$(\mathbf{v}_j - \mathbf{u}_j)^T A_{jj}\mathbf{u}_j \geq (\mathbf{v}_j - \mathbf{u}_j)^T(\mathbf{f}_j - \sum_{k \neq j} A_{jk}\,\mathbf{u}_k), \quad \mathbf{u}_j \ \mathbf{n}_j \leq g_j \ . \tag{3.8}$$

The non linear block Gauß–Seidel method gives a solution vector $\mathbf{u}_\Theta$ with respect to the modified basis $\mathbf{\Theta}$. To obtain the nodal values of the displacements $\mathbf{u}_\Phi$, we have to apply B^T, i.e., $\mathbf{u}_\Phi = B^T\mathbf{u}_\Theta$. The pre- and post processing step require two additional multiplications by B and B^T which are of lower complexity. We remark that the special structure of B yields that only a multiplication with the sparse mass matrix M has to be carried out. Additionally, the action of B can be restricted to the interface.

However, we cannot expect a better convergence rate as in the linear case which is of $\mathcal{O}(1-h^2)$, where h is the meshsize. Thus from the numerical point of view, the non linear Gauß–Seidel method does not fit our requirements. Figure 3.5 shows the convergence rates of the non linear block Gauß–Seidel method for a simple 3D example. After a few refinement steps, the convergence rate is extremely close to one. We note that due to roundoff errors, for more complex examples in 3D no convergence can be observed and the method fails. These observations motivate the introduction of our new monotone multigrid method.

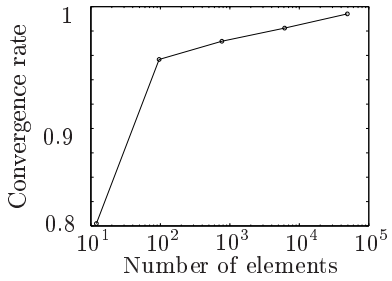

FIG. 3.5. *Convergence rate of the non linear Gauß–Seidel method for a 3D contact problem*

4. A monotone multigrid method. Monotone multigrid methods have been introduced and analyzed for variational inequalities in [26, 27, 28]. Generalization to a one-sided Signorini problem are highly nontrivial and are studied in [29, 30, 31]. One crucial property is the fact that the discrete contact condition can be satisfied locally per node. In the previous section, we have introduced a modified basis such that the multi body contact problem has formally the same algebraic structure as a one-sided Signorini problem. The main idea of this section is to apply monotone multigrid methods. These techniques combine multigrid methods with succesive energy minimization, yielding optimal iterative solvers for this type of non linear problem. The key property for the global convergence of monotone multigrid methods is the minimization of energy in each local correction step.

We assume that we have a nested sequence of triangulations $\mathcal{T}_k^i$, $i = 1, 2$, $k = 0, 1, \ldots, L$. Then the associated unconstrained product spaces $\mathbf{X}_k$ are nested, i.e., $\mathbf{X}_k \subset \mathbf{X}_{k+1}$. Unfortunately the nonconforming constrained spaces $\mathbf{V}_k$ are not nested if the triangulations are non-matching. Thus the prolongation operator from $\mathbf{V}_k$ onto $\mathbf{V}_{k+1}$ cannot be the identity. As a consequence no energy minimization can be guaranteed and monotone multigrid methods cannot be applied directly. In a first step, we consider a

local projection operator $\Pi_l(\cdot)$ from $\mathbf{X}_l$ onto $\mathbf{V}_l$

$$\Pi_l(\mathbf{v}_l) := \mathbf{v}_l - \sum_{i=1}^{d} \sum_{p \in \mathcal{P}_{C;h_s}} \frac{\int_{\Gamma_C} [\mathbf{v}_l] \cdot \mathbf{e}_i \ \psi_p \ d\sigma}{\int_{\Gamma_C} \phi_p^s \ d\sigma} \ \phi_p^s \mathbf{e}_i \ .$$

We note that $\Pi_l(\cdot)$ restricted to $\mathbf{V}_l$ is the identity. This operator has been introduced in the scalar case in [41]. Due to the biorthogonality (2.7), it is a projection. This can be easily seen by considering $\Pi_l(\Pi_l(\mathbf{v}_l))$ and using $\Pi_l(\phi_p^s \mathbf{e}_i) = 0$. Based on this projection is a modified transfer operator $(I_l^{l+1})_{\mathrm{mod}}$ from $\mathbf{V}_l$ onto $\mathbf{V}_{l+1}$ which has been introduced and analyzed in [41]. Its algebraic representation is defined in terms of the weighted mass matrix M_{l+1} on Level $l+1$

$$(I_l^{l+1})_{\mathrm{mod}} := \begin{pmatrix} \mathrm{Id} & 0 & 0 \\ 0 & \mathrm{Id} & 0 \\ 0 & M_{l+1} & 0 \end{pmatrix} I_l^{l+1} =: W_{l+1} I_l^{l+1} \ ,$$

where I_l^{l+1} is the transfer operator from $\mathbf{X}_l$ onto $\mathbf{X}_{l+1}$ with respect to the standard nodal basis Φ_l and Φ_{l+1}. We note that the unconstrained product spaces $\mathbf{X}_l$ are nested and that I_l^{l+1} is the algebraic representation of the natural embedding operator. Now, the application of the modified transfer operator is of optimal complexity. Compared with the standard transfer operator, one additional multiplication with the sparse mass matrix M_{l+1} has to be carried out. Let us consider the operator $(I_l^{l+1})_{\mathrm{mod}}$ in more detail to see why it does not fit our requirements. Observing that the algebraic representation of the linear functional $\Pi_l(\cdot)$ is W_l, we find for $\mathbf{v}_{l+1} := (I_l^{l+1})_{\mathrm{mod}} \mathbf{v}_l$

$$J(\mathbf{v}_{l+1}) = J(\Pi_{l+1}(\mathbf{v}_l)) \ .$$

From this equality, we cannot deduce that $J(\mathbf{v}_{l+1}) \leq J(\mathbf{v}_l)$. To guarantee $J(\mathbf{v}_{l+1}) \leq J(\mathbf{v}_l)$ for all $\mathbf{v}_l \in \mathbf{V}_l$, we have to define $\mathbf{v}_{l+1}$ in terms of an a-orthogonal projection operator. The application of which requires the solution of a global linear equation system with condition number $\mathcal{O}(h_{l+1}^{-2})$. On the other hand if we work with a prolongation operator which does not satisfy $J(\mathbf{v}_{l+1}) \leq J(\mathbf{v}_l)$, the monotonicity is violated, and we cannot guarantee the convergence of our method. From the numerical point of view, the solution of the global system is too expensive. Thus, we propose a different approach and introduce a nested sequence of new spaces $\widetilde{\mathbf{V}}_0 \subset \ldots \subset \widetilde{\mathbf{V}}_L$. We start by defining $\widetilde{\mathbf{V}}_L := \mathbf{V}_L$. Let $\boldsymbol{\theta}_{p,i}^l := \theta_p^l \mathbf{e}_i$ be the standard nodal basis of $\mathbf{V}_l$, then we define the new basis functions by

$$\begin{array}{rcl} \mathbf{w}_l & := & \boldsymbol{\theta}_{p,i}^l \\ \text{for } k & = & 1, \ldots, (L-l) \\ \mathbf{w}_{l+k} & := & \Pi_{l+k}(\mathbf{w}_{l+k-1}) \\ \widetilde{\boldsymbol{\theta}}_{p,i}^l & := & \mathbf{w}_L \ . \end{array} \tag{4.1}$$

It is easy to see that $\{\widetilde{\boldsymbol{\theta}}_{p,i}^l\}_{p,i}$ forms a set of linear independent functions. As a consequence, we get $\dim \mathbf{V}_l = \dim \widetilde{\mathbf{V}}_l$. Moreover by construction, we have

$$\Pi_L(\widetilde{\boldsymbol{\theta}}_{p,i}^l) = \Pi_L(\Pi_L(\mathbf{w}_{L-1})) = \Pi_L(\mathbf{w}_{L-1}) = \widetilde{\boldsymbol{\theta}}_{p,i}^l$$

and thus $\widetilde{\boldsymbol{\theta}}_{p,i}^l \in \mathbf{V}_L$. Considering the definition in more detail, we find a multiplicative structure

$$\widetilde{\boldsymbol{\theta}}_{p,i}^l = \Pi_L \circ \Pi_{L-1} \circ \ldots \Pi_{l+1} \ \boldsymbol{\theta}_{p,i}^l = \Pi_L \circ \Pi_{L-1} \circ \ldots \Pi_l \ \boldsymbol{\phi}_{p,i}^l \ ,$$

where $\boldsymbol{\phi}_{p,i}^l := \phi_p^l \mathbf{e}_i$ denotes the standard nodal hat functions on Level l associated with the nodes on the mortar side.

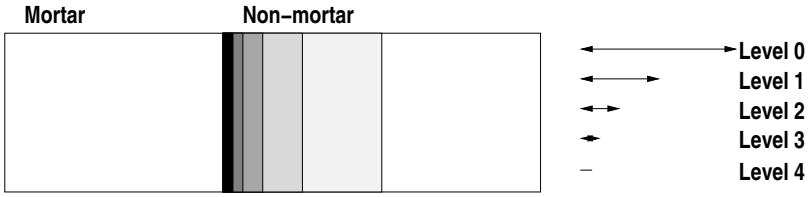

FIG. 4.1. *Multiplicative structure of the modified basis functions* $\widetilde{\boldsymbol{\theta}}^l_{p,i}$

Figure 4.1 illustrates the multilevel structure of $\widetilde{\boldsymbol{\theta}}^l_{p,i}$. On the non-mortar side corrections are added in a multiplicative way. A different possibility would be to use an additive decomposition. Since multigrid methods are multiplicative Schwarz variants, we prefer (4.1). To define the linear part of our multigrid method, we start with the construction of the prolongation operator Z_l from $\widetilde{\mathbf{V}}_l + \mathbf{S}_l$ onto $\widetilde{\mathbf{V}}_{l+1} + \mathbf{S}_{l+1}$. The algebraic presentation of $\widetilde{\boldsymbol{\theta}}^l_{p,i}$ in the nodal basis is given by

$$W_L I^L_{L-1} W_{L-1} I^{L-1}_{L-2} \dots I^{l+1}_l W_l \boldsymbol{\phi}^l_{p,i}$$

and of $\widetilde{\boldsymbol{\theta}}^{l+1}_{p,i}$ by

$$W_L I^L_{L-1} W_{L-1} I^{L-1}_{L-2} \dots I^{l+2}_{l+1} W_{l+1} \boldsymbol{\phi}^{l+1}_{p,i} \quad .$$

The last two equalities show that the prolongation from $\widetilde{\mathbf{V}}_l$ onto $\widetilde{\mathbf{V}}_{l+1}$ is given by

$$I^{l+1}_l W_l = \begin{pmatrix} (I^{l+1}_l)_{ii} & (I^{l+1}_l)_{im} + (I^{l+1}_l)_{is} M_l & 0 \\ 0 & (I^{l+1}_l)_{mm} & 0 \\ 0 & 0 & 0 \end{pmatrix} \quad .$$

We point out that the prolongation operator $I^{l+1}_l W_l$ is the algebraic representation of the natural embedding of $\widetilde{\mathbf{V}}_l$ in $\widetilde{\mathbf{V}}_{l+1}$. Figure 4.2 illustrates the prolongation operator.

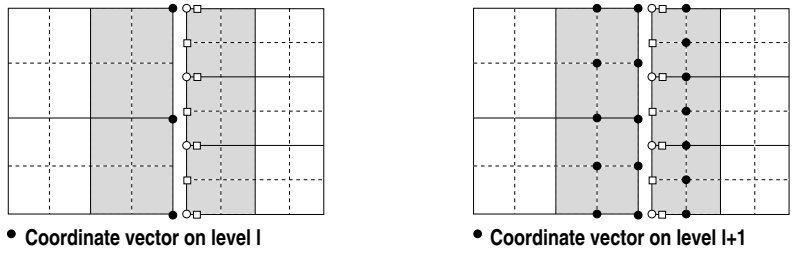

FIG. 4.2. *Prolongation operator from* $\widetilde{\mathbf{V}}_l$ *onto* $\widetilde{\mathbf{V}}_{l+1}$, $L := l+1$

For simplicity, we restrict ourselves to a function in $\widetilde{\mathbf{V}}_l$ being zero at all interior vertices. The support of such a function is marked by the shadowed region. Then, the function as an element in $\widetilde{\mathbf{V}}_l$ is uniquely defined by its values at the vertices on the mortar side which are marked by filled circles in the left picture of Figure 4.2. The values on the mortar side are extended to the non-mortar side in the defined multiplicative way such that the constraints at the interface on Level L are satisfied. The vertices on the non-mortar side on Level l are marked by empty circles and on Level $L := l+1$ by empty squares. Now, we interpret the function as an element in $\widetilde{\mathbf{V}}_{l+1}$. In the right picture, the relevant vertices to specify the function are shown by filled circles. The values at the filled circles in the interior of the non-mortar subdomain are obtained by the values at the empty circles and the standard prolongation. We note that the values at the empty squares do not contribute.

The prolongation from $\mathbf{S}_l$ onto $\widetilde{\mathbf{V}}_{l+1} + \mathbf{S}_{l+1}$ is standard. We note that $\mathbf{S}_l \not\subset \mathbf{S}_{l+1}$ but $\mathbf{S}_l \subset \mathbf{S}_{l+1} + \widetilde{\mathbf{V}}_{l+1}$. Using the fact that the prolongation Z_l is a linear mapping, we get

$$Z_l := \begin{pmatrix} (I_l^{l+1})_{ii} & (I_l^{l+1})_{im} + (I_l^{l+1})_{is} M_l & (I_l^{l+1})_{is} \\ 0 & (I_l^{l+1})_{mm} & 0 \\ 0 & 0 & (I_l^{l+1})_{ss} \end{pmatrix} . \tag{4.2}$$

We remark that the prolongation Z_l is the algebraic representation of the natural embedding $\widetilde{\mathbf{V}}_l + \mathbf{S}_l \subset \widetilde{\mathbf{V}}_{l+1} + \mathbf{S}_{l+1}$.

In a second step, we have to take care of the non linearity associated with the nodal basis functions of $\mathbf{S}_L$. Unfortunately for $l < L$, the standard nodal basis functions of $\mathbf{S}_l$ are not suitable in the non linear multigrid context. To see this, let us consider a simple two dimensional example of a curvilinear contact boundary as is depicted in Figure 4.3. Let r be a node on Level $L-1$ and let $p \neq q$ be the neighboring nodes of r on Level L.

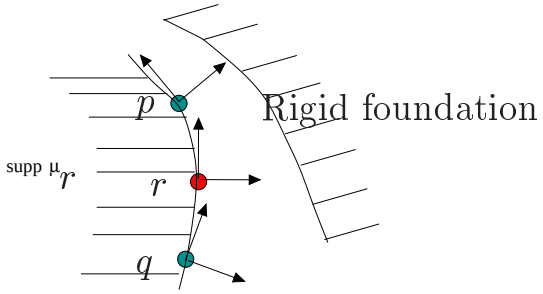

FIG. 4.3. *Coarse grid correction at curvilinear boundary*

We assume that we have different outer normals $\mathbf{n}_p \neq \mathbf{n}_q$ and that we have contact at p and q. Then, any coarse grid correction $\boldsymbol{\alpha}_r \cdot \theta_r^{L-1}$, $\boldsymbol{\alpha}_r \in \mathbb{R}^2$, has to satisfy $\boldsymbol{\alpha}_r \cdot \mathbf{n}_p = \boldsymbol{\alpha}_r \cdot \mathbf{n}_q = 0$ and thus $\boldsymbol{\alpha}_r = 0$. Using standard nodal basis functions, there is no coarse grid correction associated with the node r on Level $L-1$. As a consequence the low frequency part of the error in tangential direction at the node r cannot be handled appropriately. The additional constraints at the nodes p and q result in a reduction of the dimension of the coarse space, and the approximation property is lost. Working with the standard nodal basis of $\mathbf{S}_l$ and satisfying the constraints on Level L, we cannot guarantee anymore the optimality of the multigrid method.

Therefore, we are interested in coarse search directions which accelerate the convergence speed by generating some low-frequency sliding along the contact boundary and do not violate the non penetration condition on the finest Level L. Such type of search directions can be obtained by suitable modifications of the standard coarse grid functions. We refer to [31, 30] for the introduction of a so called *truncated* coarse grid function. We emphasize that the particular shape of the truncated coarse grid functions depends on the actual guess of the contact zone. Let us first consider the two level situation. As before in the linear setting, we introduce a modified coarse space $\tilde{\mathbf{S}}_{L-1}$, set $\tilde{\mathbf{S}}_L := \mathbf{S}_L$ and denote by $\boldsymbol{\theta}_{p,i}^L := \theta_p^L \mathbf{e}_i$ the standard nodal basis of $\mathbf{S}_L$. Then, we define the truncated basis functions by

$$\tilde{\boldsymbol{\theta}}_{p,i}^{L-1} := \boldsymbol{\theta}_{p,i}^{L-1} - \sum_{q \in \mathcal{J}_L} (\boldsymbol{\theta}_{p,i}^{L-1}(q) \cdot \mathbf{n}_q)\ \theta_q^L\ \mathbf{n}_q\,, \tag{4.3}$$

where $\mathcal{J}_L$ is the set of nodes on Level L being in contact after the leading Gauß–Seidel steps on Level L. We remark that we suppress for simplicity an additional index indicating the iteration step.

Figure 4.4 illustrates the shape of a truncated coarse grid function for given contact nodes. The given contact nodes are marked by filled circles. In the left picture, the

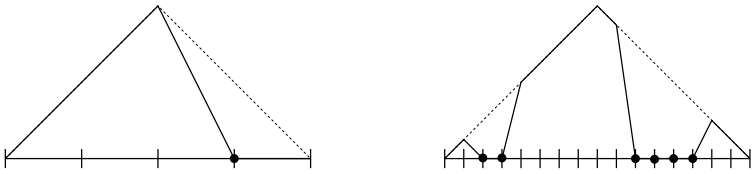

FIG. 4.4. *Two level (left) and multilevel (right) truncated coarse grid function*

two level situation is shown, and in the right picture, a multilevel situation is given. By construction, it is easy to see that $\tilde{\boldsymbol{\theta}}_{p,i}^{L-1}(q) \cdot \mathbf{n}_q = 0$ for all $q \in \mathcal{J}_L$. The construction of the truncated coarse grid functions guarantees that for each node being in contact with respect to the aczual iterate on the finest grid, the constraints are automatically satisfied, and no correction in normal direction occurs. As a consequence, we do not obtain additional constraints, and the dimension of the modified coarse grid spaces $\tilde{\boldsymbol{S}}_{L-1}$ is not reduced in tangential direction.

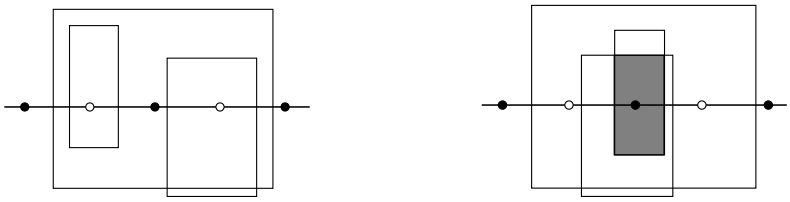

FIG. 4.5. *Local box constraints $\tilde{\mathcal{K}}_l(p)$ on Level l (left) and $\tilde{\mathcal{K}}_{l-1}(p)$ Level $l-1$ (right)*

Unfortunately, it is not sufficient to construct coarse grid functions satisfying the constraints for all p being at the actual iterate in contact. To guarantee that a new iterate is in the convex set $\mathcal{K}_L$, it is not sufficient to verify one constraint per node on Level $l < L$. Additionally, we have to satisfy all constraints on Level L being not at the actual iterate in contact. Using uniform refinement, we obtain $\mathcal{O}(2^{(d-1)(L-l)})$ constraints for each node p on Level l. As a consequence, the optimal complexity of the algorithm is lost and a logarithm occurs. To avoid this, we use modified convex sets. In a first step, we introduce convex sets depending on the actual iterate. We define for a given convex set $\mathcal{D}_l$ on Level $l < L$ and a given vector $\mathbf{z}_l$, the convex set $\mathcal{P}_l(\mathbf{z}_l, \mathcal{D}_l) := \{\mathbf{v}_l | \mathbf{v}_l + \mathbf{z}_l \in \mathcal{D}_l\}$. Moreover, we define the restriction of a given convex set $\mathcal{D}_l$ on Level $l \leq L$ in terms of local box constraints such that $\mathcal{D}_{l-1} := R_l \mathcal{D}_l \subset \mathcal{D}_l$, see [28, 31]. More precisely, the constraints for $\mathcal{D}_{l-1}$ are only associated with the nodes on Level $l-1$. Let $\mathcal{D}_l$ be the actual convex set defined by local box constraints $\mathcal{B}_p^l := [\alpha_1^{p;l}, \beta_1^{p;l}] \times \ldots \times [\alpha_d^{p;l}, \beta_d^{p;l}]$, $\alpha_i^{p;l} \in [-\infty, 0]$, $\beta_i^{p;l} \in [0, \infty]$, $1 \leq i \leq d$, for each node p on the non-mortar side on Level l. Then, we define $R_l \mathcal{D}_l$ by local box constraints $\mathcal{B}_p^{l-1} := [\alpha_1^{p;l-1}, \beta_1^{p;l-1}] \times \ldots \times [\alpha_d^{p;l-1}, \beta_d^{p;l-1}]$ for each node p on the non-mortar side on Level $l-1$. We set

$$\alpha_i^{p;l-1} := \max_{q \in \mathcal{J}_p} (\alpha_i^{q;l}) \,, \quad \beta_i^{p;l-1} := \min_{q \in \mathcal{J}_p} (\beta_i^{q;l}) \quad ,$$

where $\mathcal{J}_p$ is set of nodes q on Level l such that q and p are vertices of one boundary face on Level l. On the finest Level L, we define for a given $\mathbf{z}_L \in \mathcal{K}_L$ the convex set $\mathcal{P}_L(\mathbf{z}_L \in \mathcal{K}_L)$ by local box constraints $\mathcal{B}_p^L$ with

$$\alpha_i^{p;L} := -\infty \,, \quad \beta_i^{p;L} := d^{-1}(g_p - \mathbf{z}_L(p) \cdot \mathbf{n}_p)/(\mathbf{n}_p)_i \,.$$

if $(\mathbf{n}_p)_i > 0$ and

$$\alpha_i^{p;L} := d^{-1}(g_p - \mathbf{z}_L(p) \cdot \mathbf{n}_p)/(\mathbf{n}_p)_i \,, \quad \beta_i^{p;L} := \infty \,,$$

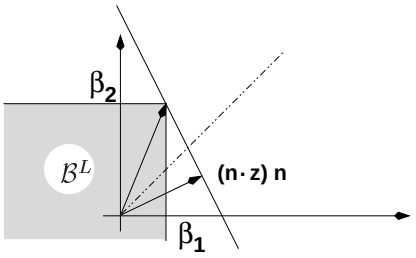

FIG. 4.6. *Construction of box constraints on Level L*

if $(\mathbf{n}_p)_i < 0$ and $\alpha_i^{p;L} := -\infty\,, \quad \beta_i^{p;L} := \infty$ if $(\mathbf{n}_p)_i = 0$, see Figure 4.6.

For more sophisticated strategies, we refer to [31, 28]. It can be easily seen that $\mathbf{z}_L + \mathbf{w}_L \in \mathcal{K}_L$ for $\mathbf{w}_L \in \mathcal{P}_L(\mathbf{z}_L, \mathcal{K}_L)$. We note that in general $\mathcal{P}_L(\mathbf{z}_L, \mathcal{K}_L)$ is a true subset of $\{\mathbf{w}_L \,|\, \mathbf{w}_L + \mathbf{z}_L \in \mathcal{K}_L\}$. Now, we are ready to define our truncated coarse basis recursively. We start with $\tilde{\boldsymbol{\theta}}^L := \boldsymbol{\theta}^L$ and set

$$\tilde{\boldsymbol{\theta}}^l := (I_{l+1}^l)_{ss} P_{l+1} \tilde{\boldsymbol{\theta}}^{l+1}, \quad l = L-1, L-2, \ldots, 0\ ,$$

where P_{l+1} is a $dn_s^{l+1} \times dn_s^{l+1}$ block matrix depending on the actual iterate. Here, n_s^{l+1} stands for the number of vertices on Level $l+1$ on the non-mortar side. The $d \times d$ block matrices are associated with the nodes p on Level $l+1$ on the non-mortar side. On Level $l+1 = L$, they are given by

$$\mathrm{Id} - \omega_p \mathbf{n}_p \mathbf{n}_p^T$$

and we set $\omega_p = 1$ if $\mathbf{z}_L(p) \cdot \mathbf{n}_p = g_p$ and $\omega_p = 0$ otherwise. On the lower levels $l+1 < L$, the truncation strategy is slightly different. Here, truncation is not restricted to one direction. For a given $\mathbf{z}_l \in \mathcal{D}_l$, truncation is applied whenever $\mathbf{z}_l(p)$ touches the boundary of the local box constraint. We set

$$\mathrm{Id} - \sum_{i=1}^{d} \omega_{p,i} \mathbf{e}_{p,i} \mathbf{e}_{p,i}^T\ ,$$

where $\omega_{p,i} = 1$, if the local correction at the node p is on the boundary of the convex set $\mathcal{B}_p^{l+1}$ in direction $\mathbf{e}_i$ and $\omega_{p,i} = 0$ otherwise. The truncations strategies being different reflects the fact that only on the finest grid we have to take care of the normal directions. We note that P_{l+1} is the identity if the actual iterate is in the interior of the (restricted) convex set. Combining this non linear restriction operator with our linear one given by the transposed of the prolongation (4.2), we define

$$\tilde{Z}_l^T := \begin{pmatrix} (I_{l+1}^l)_{ii} & 0 & 0 \\ (I_{l+1}^l)_{mi} + M_l^T (I_{l+1}^l)_{si} & (I_{l+1}^l)_{mm} & 0 \\ (I_{l+1}^l)_{si} & 0 & (I_{l+1}^l)_{ss} P_{l+1} \end{pmatrix}\ .$$

In terms of this new non linear restriction operator, we formulate our iterative scheme $\mathbf{u}_L^{n+1} := \mathrm{MG}(L, A_L, f_L, \mathbf{u}_L^n, \mathcal{K}_L, m_1, m_2)$ as $\mathcal{V}$-cycle multigrid method with m_1 pre- and m_2 postsmoothing steps. The start iterate $\mathbf{u}_L^0$ is given. We denote by $\mathrm{GS}(A, d, \mathbf{v}, \mathcal{D}, k)$ the k-th iterate of the non linear Gauß–Seidel method applied to the start iterate $\mathbf{v}$ with matrix A, right hand side d and constraint set $\mathcal{D}$.

MONOTONE MULTIGRID ALGORITHM: $\mathrm{MG}(l, \tilde{A}_l, d_l, \mathbf{v}_l, \tilde{\mathcal{D}}_l, m_1, m_2)$

Presmoothing: $\mathbf{z}_l^1 := \mathrm{GS}(\tilde{A}_l, d_l, \mathbf{v}_l, \tilde{\mathcal{D}}_l, m_1)$

Coarse grid correction:

$$\begin{aligned}
&\tilde{A}_{l-1} := \tilde{Z}_l^T \tilde{A}_l \tilde{Z}_l \\
&d_{l-1} := \tilde{Z}_l^T (d_l - \tilde{A}_l \mathbf{z}_l^1) \\
&\tilde{\mathcal{D}}_{l-1} := R_l \mathcal{P}_l(\mathbf{z}_l^1, \tilde{\mathcal{D}}_l) \\
&\text{if } l > 1,\ \mathbf{q}_{l-1} := \mathrm{MG}(l-1, \tilde{A}_{l-1}, d_{l-1}, \mathbf{0}, \tilde{\mathcal{D}}_{l-1}, m_1, m_2) \\
&\text{else} \qquad \mathbf{q}_0 := \mathrm{GS}(0, \tilde{A}_0, d_0, \mathbf{0}, \tilde{\mathcal{D}}_0, \infty)
\end{aligned}$$

Prolongation: $\mathbf{z}_l^2 := \mathbf{z}_l^1 + \tilde{Z}_l \mathbf{q}_{l-1}$

Postsmoothing: $\mathrm{MG}(l, \tilde{A}_l, d_l, \mathbf{v}_l, \tilde{\mathcal{D}}_l, m_1, m_2) := \mathrm{GS}(\tilde{A}_l, d_l, \mathbf{z}_l^2, \tilde{\mathcal{D}}_l, m_2)$.

On the coarsest level, the resulting constrained problem is solved up to a given tolerance by suitably many steps of the non linear Gauß–Seidel method. This is denoted by the ficticious iteration number ∞. In case of a coarse grid with many degrees of freedom, an equally modified algebraic multigrid method can be applied. For a numerical result, we refer to the 3D example in Section 5. We remark that the restriction $\tilde{Z}_l$ depends on $\mathbf{z}_l^1$, see also [31]. In our implementation, the coarse grid matrices are only locally reassembled if a change of phase occurs. The definition of R_l guarantees that the prolongated correction is in $\mathcal{P}_l(\mathbf{z}_l^1, \tilde{\mathcal{D}}_l)$ and thus $\mathbf{z}_l^2 \in \mathcal{D}_l$.

Our definition of the truncated search directions give rise to local corrections which are admissible with respect to the *actual guess* of the contact boundary. The corresponding non linear $\mathcal{W}$-cycle multigrid algorithm is straightforward.

THEOREM 4.1. *Under suitable assumptions, our monotone multigrid algorithm is globally convergent. Moreover, the discrete contact boundary is identified after a finite number of iteration steps.*

In [30, 31], the global convergence of a truncated monotone multigrid method for a one-sided Signorini problem has been shown. Moreover, under some stability assumption, it is also shown that in this case the discrete contact boundary is detected after a finite number of iteration step. Due to the decomposition (3.5), these results do also apply for our monotone method. We refer to [31, Theorem 3.9] for details.

5. Numerical Results in 2D and 3D. In this section, we present numerical results in 2D and 3D illustrating the performance of our new method for elastic contact problems. Moreover, we compare our new non linear method with a standard linear multigrid method. To this end, the boundary stresses computed by means of our monotone multigrid method are taken as boundary data for the standard linear multigrid method. As it turns out, the convergence rates of our new non linear and of the linear multigrid method are almost the same. With respect to execution time, there is no significant difference between our non linear multigrid method applied to a contact problem and the standard multigrid method applied to the corresponding linear problem with known boundary stresses. Our non linear method has been implemented in the framework of the finite element toolbox UG, see [2]. The implementation of the non linear method is based on the abstract obstacle problem class developed in [31] in the context of one-sided contact problems.

The first example to be considered is a frictionless Hertzian contact problem of a disc with a plane in 2D. The problem data is taken from [9] where a penalty method is applied to the contact problem. For this example, the boundary stresses are given analytically, see [18], and we can compare the computed boundary stresses with the analytical ones. On top of the disc, Dirichlet boundary conditions are applied corresponding to a point load of $F = 100N$. The coarse grid, see the left picture of Figure 5.1, has been generated using a grid generator. During the adaptive refinement process, new boundary nodes are moved to their position on the boundary of the disc.

The plane is modeled by a rectangle with homogeneous Dirichlet boundary conditions

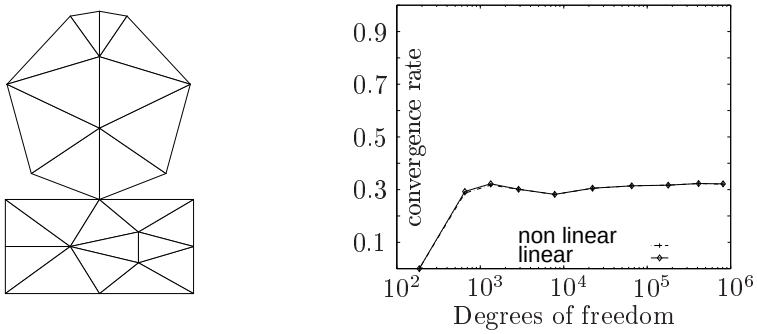

FIG. 5.1. *2D example: Coarse grid and comparison of non linear and linear method*

on the left and the right side. Homogeneous Neumann boundary conditions are applied elsewhere. We use different materials for the plane and the disc and take $E = 10^6$ and $\nu = 0.45$ for the plane and $E = 7000$ and $\nu = 0.3$ for the disc. On each level, the arising discrete system is solved up to a given tolerance of $\varepsilon_{\mathrm{TOL}} = 10^{-11}$, e.g., the iteration process on Level l is stopped if

$$a(\mathbf{u}_l^n - \mathbf{u}_l^{n-1}, \mathbf{u}_l^n - \mathbf{u}_l^{n-1})^{1/2} \leq \varepsilon_{\mathrm{TOL}}\,. \tag{5.1}$$

We denote the final iterate by $\mathbf{u}_l^{n_l}$. To measure the performance of our new monotone multigrid method, the computed boundary stresses are taken as boundary data for a standard linear multigrid method. In both cases, we chose $\mathbf{u}_l^0 = 0$ on each Level l, use (5.1) as stopping criteria and apply a $\mathcal{W}(3,3)$–cycle. The asymptotic linear convergence rates are defined by

$$\rho_l^2 = \frac{a(\mathbf{u}_l^{n_l} - \mathbf{u}_l^{n_l-1}, \mathbf{u}_l^{n_l} - \mathbf{u}_l^{n_l-1})}{a(\mathbf{u}_l^{n_l-1} - \mathbf{u}_l^{n_l-2}, \mathbf{u}_l^{n_l-1} - \mathbf{u}_l^{n_l-2})}\,.$$

We emphasize, that the iteration process of our monotone multigrid method takes care of the non linearity at the contact boundary. Due to the modifications, we observe an increase of about 10 % of the cpu time on each level. The asymptotic convergence rates of our non linear (crosses) and of the linear (diamonds) multigrid method vs. the number of unknowns are given in the right picture of Figure 5.1. We observe level independent convergence rates. Moreover, the asymptotic convergence rates are for both methods are the same.

Level l	n_l	# iterations monotone	# iterations standard	# contact nodes
0	186	4	4	1
1	654	20	20	3
2	1.336	22	22	3
3	2.874	22	21	7
4	7.794	21	21	13
5	22.132	22	22	27
6	65.208	23	23	53
7	178.598	24	24	105
8	412.430	24	24	209
9	811.030	24	24	417

TABLE 5.1

2D example: Non linear method for unknown contact boundary vs. linear method for known contact boundary data for the Hertzian contact problem

Table 5.1 shows the number of required iterations n_l on each Level l for both methods. As can be seen, the number of iterations is bounded independently of the refinement level. For almost all refinement levels, the numbers are the same.

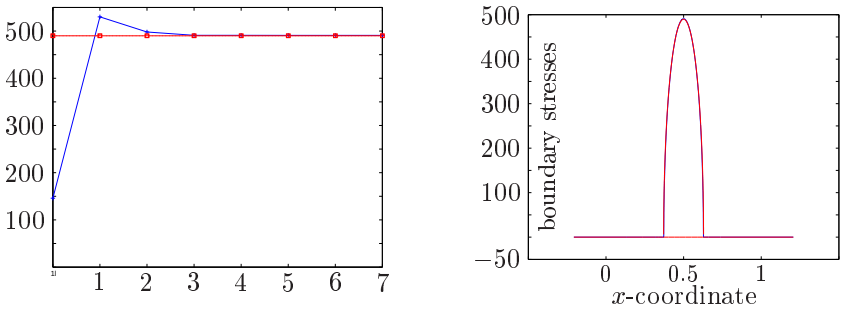

FIG. 5.2. *Hertzian contact problem (2D): Maximal contact stresses on Level* $0, \ldots, 7$ *(left) and boundary stresses on Level* 9 *(right)*

The final approximation of the boundary stresses on Level $L = 9$ can be seen in the right picture of Figure 5.2. Here, the approximation of the contact stresses obtained using our new monotone method is plotted. We note that the horizontal line is the computed tangential stresses. The use of vector valued dual Lagrange multipliers to approximate the stresses yields very accurate results. In particular, the tangential stress is an additional unknown. Thus, our approach can be easily generalized to multi body contact problems including friction. In the left picture of Figure 5.2, the maximal boundary stresses computed on each level and the theoretical value (horizontal line with squares) of the maximal boundary stresses is depicted. On Level 3, the error of the maximal boundary stress with respect to the analytical solution is 0.016% and on Level 4 only 0.002%. This corresponds to 7 and 13 nodes being in contact with the plane, see Table 5.1.

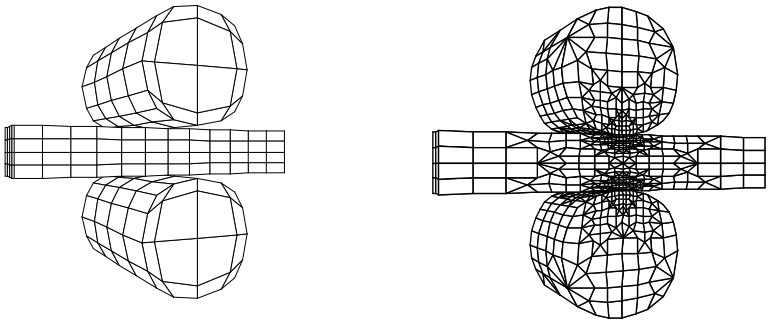

FIG. 5.3. *3D example: Corse grid (left) and refined grid (right)*

In 3D, we reconsider the example given in Section 3. The geometry consists of two rollers and a bar and is depicted in Figure 3.1. Inhomogeneous Dirichlet boundary conditions are applied on the upper and lower part of the upper and lower roller, respectively, pressing the two rollers against the bar. Homogeneous Neumann boundary conditions are applied elsewhere. In a first step, we apply our new monotone method for elastic contact. In contrast to the Dirichlet–Neumann method, see Figure 3.2, no oscillation occurs. This is due to the fact that our method is monotone and global convergence is guaranteed. The final approximation of the geometry using adaptive refinement can be seen in the right picture of Figure 5.3. In the left picture of Figure 5.3, the coarse grid is shown.

In Table 5.2, we compare the performance of our new non linear method with a standard multigrid method applied to the linear problem. The required iteration numbers needed to achieve the given tolerance $\varepsilon_{\mathrm{TOL}} = 10^{-7}$ are reported. For both methods,

level	n_k	# iterations monotone	# iterations standard	# contact
0	1.725	2	2	10
1	5.253	11	11	18
2	10.191	12	22	34
3	23.799	13	25	198
4	38.487	24	23	514
5	75.045	12	19	1.630

TABLE 5.2
3D example: Non linear method for unknown contact boundary vs. linear method for known boundary data

nested iteration is used. As can be seen, the non linear method behaves as well as the standard multigrid method.

We use trilinear finite elements on hexahedrons. Although these kinds of elements are well suited for the numerical approximation of elastic materials, the aspect ratio of the elements situated at the boundary of the cylinders does depend on the level. For this reason, our method is accelerated by a conjugated gradient method, once the contact boundary has been identified. Additionally, the inner nodes of the grids are moved after each refinement step to improve the grid quality. Proceeding in this way, it is possible to compensate the influence of the badly shaped elements at the boundary. We remark, that it is also possible to use tetrahedrons or prisms instead of hexahedrons. However, hexahedrons usually give rise to a better approximation of the displacements and boundary stresses. Since on the coarse grid we have 1.725 unknowns, we do not use a non linear Gauss–Seidel method as coarse grid solver. Instead, we apply an algebraic monotone multigrid method.

REFERENCES

[1] H. BADER AND R. HOPPE, *Multigrid solution of Signorini type problems in contact elastostatics.*, Tech. Rep. TUM–M9304, TU München, 1993.

[2] P. BASTIAN, K. BIRKEN, K. JOHANNSEN, S. LANG, N. NEUSS, H. RENTZ-REICHERT, AND C. WIENERS, *UG – a flexible software toolbox for solving partial differential equations.*, Computing and Visualization in Science, 1 (1997), pp. 27–40.

[3] F. BEN BELGACEM, *The mortar finite element method with Lagrange multipliers*, Numer. Math., 84 (1999), pp. 173–197.

[4] F. BEN BELGACEM, P. HILD, AND P. LABORDE, *Approximation of the unilateral contact problem by the mortar finite element method*, C. R. Acad. Sci., Paris, Ser. I, 324 (1997), pp. 123–127.

[5] ———, *Extension of the mortar finite element method to a variational inequality modeling unilateral contact*, Math. Models Methods Appl. Sci., 9 (1999), pp. 287–303.

[6] C. BERNARDI, Y. MADAY, AND A. PATERA, *Domain decomposition by the mortar element method*, in In: Asymptotic and numerical methods for partial differential equations with critical parameters, H. K. et al., ed., Reidel, Dordrecht, 1993, pp. 269–286.

[7] C. BERNARDI, Y. MADAY, AND T. PATERA, *A new nonconforming approach to domain decomposition: The mortar element method*, in Nonlinear Partial Differential Equations and Their Applications, H. Brezis and J. L. Lions, eds., Pitman, 1994, pp. 13–51.

[8] P. BOIERI, F. GASTALDI, AND D. KINDERLEHRER, *Existence, uniqueness and regularity results for the two–body contact problem*, Applied Mathematics and Optimzation, 15 (1987), pp. 251–227.

[9] C. CARSTENSEN, O. SCHERF, AND P. WRIGGERS, *Adaptive finite elements for elastic bodies in contact*, SIAM J. Sci. Comp., 20 (1999), pp. 1605–1626.

[10] P. COOREVITS, P. HILD, AND J.-P. PELLE, *A posteriori error estimation for unilateral contact with matching and non-matching meshes*, Comput. Methods Appl. Mech. Eng., 186 (2000), pp. 65–83.

[11] Z. DOSTÁL, *Box constrained quadratic programming with proportioning and projections.*, SIAM J. Optim., 7 (1997), pp. 871–887.

[12] P. EBERHARD, *Kontaktuntersuchungen durch hybride Mehrkörpersystem/Finite Elemente Simulationen*, Shaker Verlag, 2000.

[13] C. ECK, O. STEINBACH, AND W. WENDLAND, *A symmetric boundary element method for contact*

problems with friction, Mathematics and Computers in Simulation, 50 (1999), pp. 43–61.

[14] R. Glowinski, *Numerical Methods for Nonlinear Variational Problems*, Series in Computational Physics, Springer, New York, 1984.

[15] W. Hackbusch and H. Mittelmann, *On multigrid methods for variational inequalities*, Numer. Math., 42 (1983), pp. 65–76.

[16] J. Haslinger and I. Hlaváček, *Contact between elastic bodies. I. continuous problems*, Apl. Mat., 25 (1980), pp. 324–327.

[17] ———, *Contact between elastic bodies. II. finite element analysis.*, Apl. Mat., 26 (1981), pp. 263–290.

[18] H. Hertz, *Über die Berührung fester elastischer Körper*, J.f. Math., 92 (1882).

[19] P. Hild, *A propos d'approximation par éléments finis optimale pour les problémes de contact unilatéral*, C. R. Acad. Sci., Paris, Ser. I, 330 (1998), pp. 1233–1236.

[20] ———, *Numerical implementation of two nonconforming finite element methods for unilateral contact*, Comput. Methods Appl. Mech. Eng., 184 (2000), pp. 99–123.

[21] R. Hoppe, *Multigrid algorithms for variational inequalities*, SIAM J. Numer. Anal., 24 (1987), pp. 1046–1065.

[22] R. Hoppe and R. Kornhuber, *Adaptive multilevel–methods for obstacle problems.*, SIAM J. Numer. Anal., 31 (1994), pp. 301–323.

[23] J. N. I. Hlaváček, J. Haslinger and J. Lovíšek., *Solution of variational inequalities in mechanics*, Springer, Berlin, 1988.

[24] N. Kikuchi and J. Oden, *Contact problems in elasticity: A study of variational inequalities and finite element methods*, SIAM Studies in Applied Mathematics 8, Philadelphia, 1988.

[25] C. Kim, R. Lazarov, J. Pasciak, and P. Vassilevski, *Multiplier spaces for the mortar finite element method in three dimensions*, Preprint, Texas A&M University, (2000). submitted.

[26] R. Kornhuber, *Monotone multigrid methods for elliptic variational inequalities I*, Numer. Math., 69 (1994), pp. 167–184.

[27] ———, *Monotone multigrid methods for elliptic variational inequalities II*, Numer. Math., 72 (1996), pp. 481–499.

[28] ———, *Adaptive monotone multigrid methods for nonlinear variational problems*, Teubner–Verlag, Stuttgart, 1997.

[29] R. Kornhuber and R. Krause, *On monotone multigrid methods for the Signorini problem*, in Numerical Techniques for Composite Materials, W. Hackbusch and S. Sauter, eds., Proceedings of the 15th GAMM Seminar Kiel, 1999. in preparation.

[30] ———, *Adaptive multigrid methods for Signorini's problem in linear elasticity.* to appear in Computing and Visualization in Science, 2001.

[31] R. Krause, *Monotone Multigrid Methods for Signorini's Problem with Friction*, PhD thesis, FU Berlin, 2001.

[32] R. Krause and B. Wohlmuth, *A Dirichlet–Neumann type algorithm for contact problems with friction*, tech. rep., FU Berlin, 2001.

[33] P. Le Tallec, *Handbook of Numerical Analysis*, vol. III, Nort–Holland, 1994, ch. Numerical Methods for Nonlinear Three-Dimensional Elasticity. P.G. Ciarlet and J.L. Lions *(Eds.)*.

[34] P. Oswald and B. Wohlmuth, *On polynomial reproduction of dual FE bases*, in Thirteenth International Conference on Domain Decomposition Methods, N. Debit, M. Garbey, R. Hoppe, J. Pèriaux, D. Keyes, and Y. Kuznetsov, eds., 2001, pp. 85–96.

[35] G. Pietrzak and A. Curnier, *Large deformation frictional contact mechanics: continuum formulation and augmented Lagrangian treatment*, Computer Methods in Applied Mechanics and Engeneering, 177 (1999), pp. 351–381.

[36] J. L. R. Glowinski and J. Trémolières, *Numerical analysis of variational inequalities*, North–Holland, Amsterdam, 1981.

[37] J. Schöberl, *Efficient contact solvers based on domain decomposition techniques*, Computers & Mathematics with Applications, 42 (2001), pp. 1217–1228.

[38] K. Willner and L. Gaul, *Contact description by fem based on interface physics*, in Computational Plasticity V, Barcelona, Spain, 1997.

[39] B. Wohlmuth, *A mortar finite element method using dual spaces for the Lagrange multiplier*, SINUM, 38 (2000), pp. 989–1014.

[40] ———, *A comparison of dual Lagrange multiplier spaces for mortar finite element discretizations*, tech. rep., submitted, 2001.

[41] ———, *Discretization Methods and Iterative Solvers Based on Domain Decomposition*, vol. 17 of Lecture Notes in Computational Science and Engeneering, Springer Heidelberg, 2001.

[42] P. Wriggers, *Finite element algorithms for contact problems*, Arch. Comp. Meth. Engrg., 2 (1995), pp. 1–49.

[43] P. Wriggers, *Finite elements for the thermomechanical contact and adaptive finite element analysis of contact problems.*, in New developments in contact problems., CISM Courses Lect., Springer, 1999, pp. 179–246.